Internal Waves in the Arctic Ocean: Comparison with Lower-Latitude Observations

MURRAY D. LEVINE AND CLAYTON A. PAULSON

College of Oceanography, Oregon State University, Corvallis, OR 97331

JAMES H. MORISON

Polar Science Center, University of Washington, Seattle, WA 98195

(Manuscript received 13 April 1984, in final form 13 November 1984)

ABSTRACT

A thermistor chain was moored below the pack ice from 50–150 m in the Arctic Ocean for five days in 1981. Oscillations in temperature are attributed to the vertical displacement of internal waves. The spectral shape of isotherm displacement is consistent with the Garrett-Munk model and other internal wave observations, but the spectral level is significantly lower. Other observations from the Arctic Ocean also exhibit lower internal-wave energy when compared with historical data from lower latitudes. The lower energy may be related to the unique generation and dissipation mechanisms present in the ice-covered Arctic Ocean. Significant peaks in vertical coherence occur at 0.81 and 2.6 cph. The peak at 2.6 cph coincides approximately with the high-frequency spectral cutoff near the local buoyancy frequency; this feature has been observed in many other internal wave experiments. The coherent oscillations at 0.81 cph exhibit a node in vertical displacement at 75–100 m. This is consistent with either the second, third or fourth vertical mode calculated from the mean buoyancy frequency profile. Evidence is presented which suggests that, contrary to the Garrett-Munk model, the frequency spectrum does not scale with the Coriolis parameter.

1. Introduction

The internal wave field in the mid-latitude ocean is remarkably steady and uniform. This observation motivated Garrett and Munk's universal isotropic model of the internal wave spectrum (Garrett and Munk, 1972; 1975; hereafter referred to as GM). The GM model has served as a useful framework for the analysis and comparison of internal wave observations. While the kinematic description of the internal wave field has continued to improve, our understanding of the physical processes that generate and dissipate the waves remains woefully inadequate (e.g., Olbers, 1983; Levine, 1983).

Wunsch (1975) suggested that deviations of internal wave spectra from universal form may provide clues to sources and sinks of internal waves. However, the identification of variations in the wave field caused by variations in forcing and dissipation has proved difficult. The extensive measurements made during the Internal Wave Experiment (IWEX) agree reasonably well with the GM model except for a peak at low wavenumber and a decrease in the number of modes at high frequency (Müller *et al.*, 1978). Many upper-ocean observations also exhibit a positive deviation from the GM spectrum at high frequency accompanied by an increase in vertical coherence (e.g. Pinkel, 1975; Levine *et al.*, 1983a,b; Käse and Siedler, 1980). Roth *et al.* (1981) found that internal wave spectral levels in the upper ocean tended to fluctuate above the level of the GM spectrum. The influence of the internal tide and its harmonics on the remainder of the spectrum is uncertain (e.g., Pinkel, 1981; Levine *et al.*, 1983b). Better documentation of the temporal variations in the internal wave field with long time series is just beginning (e.g., Briscoe and Weller, 1984). Regions of anomalously high internal wave energy near topographic features have been identified but are apparently due to the kinematic readjustment of the wave field from reflection off the bottom (Eriksen, 1982) or focusing in canyons (Hotchkiss and Wunsch, 1982). In summary, the link between a generation mechanism and observed high energy has not been conclusively established. Perhaps by compiling many more observations in varied environments significant correlation between the wave field and other processes will be found.

In the search for deviations from the universality of the internal wave spectrum, a modest experiment was performed in the Arctic Ocean in May 1981 north of Spitzbergen during the occupation of the FRAM 3 ice camp. A thermistor chain was moored from the ice and time series of vertical displacement of isotherms were obtained. The purpose of this paper is to present the results of an analysis of these observations and to compare spectra and vertical coherence with other Arctic and lower-latitude observations of internal waves. The GM model is used as

a convenient framework to aid in making the comparisons. Specifically, we compare spectral energy levels scaled by buoyancy frequency. In addition, the effect of eliminating the Coriolis parameter from the GM scaling is tested.

2. Observations

A single Aanderaa thermistor chain was moored from the pack ice for five days beginning on 1 May, 1981, at 81°50'N, 5°10'E, north of Spitzbergen over the Yermak Plateau (Fig. 1). At the time of recovery on 6 May the mooring had drifted 24 km to the west at an average rate of 7 cm s^{-1}. The chain recorded temperature every 2 minutes at 10 m intervals over a depth range of 49–149 m. Pressure was measured at 48 m to determine the amount of tilt of the mooring caused by the relative velocity between the water and ice.

The sensors were placed in the nearly uniform temperature gradient between the relatively cold Arctic surface water and the deeper warm Atlantic water (Coachman and Aagaard, 1974). Temperature and salinity profiles measured with the APS, profiling current meter–CTD (Morison, 1980), are shown in Fig. 2. The mooring depth was chosen to insure that a large temperature signal would result from any significant vertical displacement of the water. The Aanderaa data logger was modified to record at a resolution of 0.005°C, which corresponds to a vertical displacement of 15 cm in this temperature gradient. The density field over this depth range is dominated by salinity, but the T–S relationship was stable enough during this period to tag a density surface by its temperature.

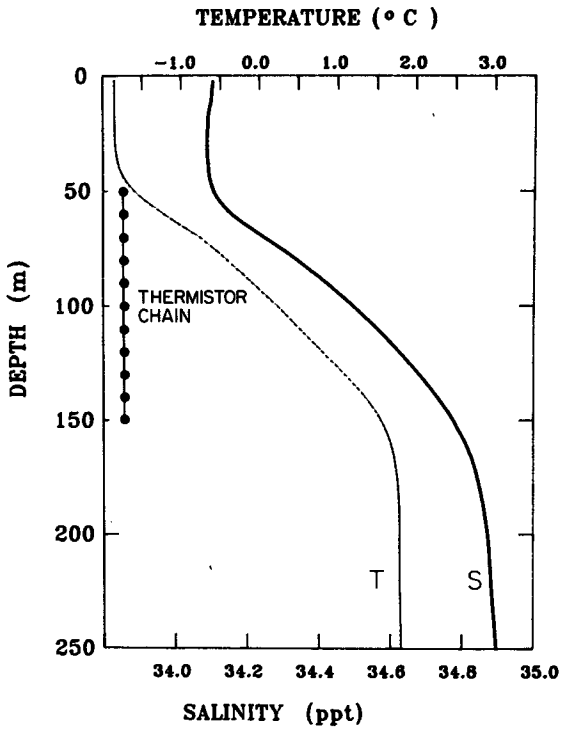

FIG. 2. Average vertical profiles of temperature (thin line) and salinity (bold line) from 20 casts of the APS, profiling current meter-CTD, made concurrently with the thermistor chain deployment. The location of the thermistor chain is indicated.

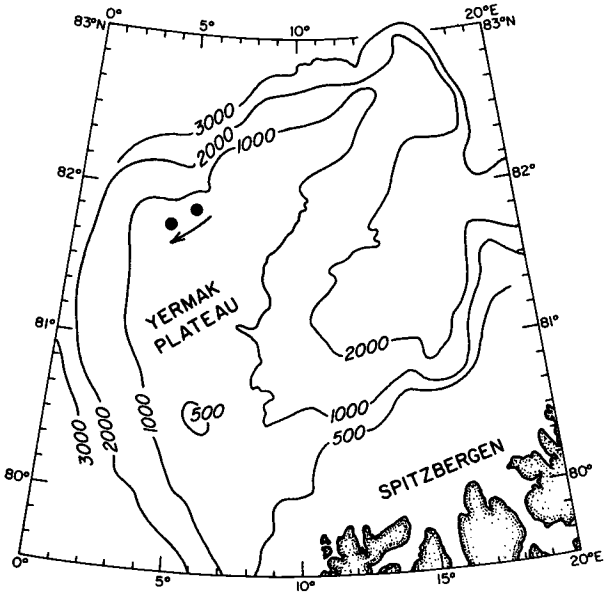

FIG. 1. Map showing the positions of FRAM 3 ice camp (solid dots) at the times of the deployment and recovery of the thermistor chain 5 days later. Bathymetric data, contoured in meters, are from Jackson *et al.* (1984).

Time series of isotherm depth were calculated by linearly interpolating the position of a given isotherm between the appropriate pair of thermistors. The vertical positions of the thermistors were assumed constant because the recorded pressure variation was always less than the 20 cm resolution of the pressure sensor. Sixteen time series of isotherm depth in increments of 0.2°C were obtained. An example of a one-day record of the series is shown in Fig. 3.

The series of isotherm depth were divided into two time segments and pre-whitened by applying a first-difference filter to reduce spectral leakage. Fourier transforms were computed, and the resulting spectra were recolored to restore the signal removed by the filter. Smoothed estimates of auto- and cross-spectra were formed by ensemble-averaging the spectra from the two segments and averaging in non-overlapping frequency bands, equally spaced on a logarithmic frequency scale. Vertical displacement spectra are shown in Fig. 4a for the −0.8° and 1.6°C isotherms which oscillated around average depths of 67 and 137 m, respectively. Vertical coherence estimates between the isotherms at mean depths of 57 and 76 m are shown in Fig. 5.

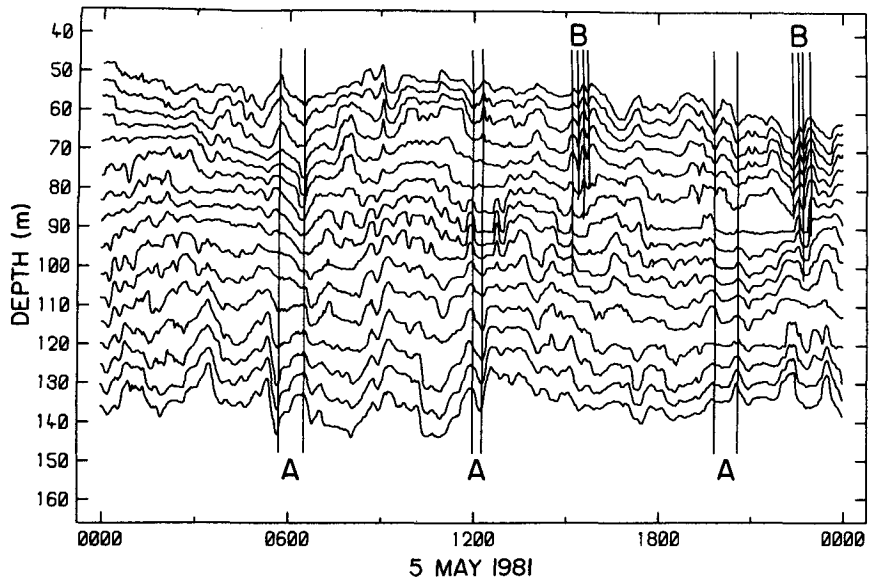

FIG. 3. Isotherm depths as a function of time on 5 May 1981. The 16 isotherms shown are in intervals of 0.2° from −1.4° (shallowest) to 1.6° (deepest). Examples of oscillations that are responsible for the high coherence in the frequency band around 0.81 cph are labeled A. Note the presence of a node at 75–100 m. Higher-frequency fluctuations that contribute to the high coherence at 2.6 cph are labeled B.

A representative vertical profile of the buoyancy frequency $N(z)$ was spliced together from two data sources (Fig. 6). Values in the upper 250 m were obtained by averaging 20 profiles recorded by the CTD during the time the mooring was deployed. The buoyancy frequency increases with depth to a peak of 4 cph at about 75 m followed by a monotonic decrease. Below 250 m values were calculated from water samples taken by scientists from the Lamont-Doherty Geological Observatory (Manley, personal communication, 1982). In this region N was a nearly uniform 1 cph.

3. Spectrum

Frequency spectra of isotherm displacement from 67 and 137 m are presented in Fig. 4a. In the internal wave band between the inertial frequency, f (0.0825 cph), and the local buoyancy frequency N the spectral slopes are between −1.5 and −2.0. To accentuate the internal wave band, the displacement spectra were converted to vertical velocity spectra by multiplying by the square of the frequency (Fig. 4b). A spectral roll-off occurs at frequencies above local N. The spectrum at 67 m is generally lower than the one at 137 m. When the spectra are scaled by multiplying by the local value of N, the difference between the spectra is reduced (Fig. 4c). This is consistent with the $1/N$ scaling of vertical displacement that follows by assuming that $N(z)$ is a "slowly" varying function (WKB approximation).

The spectral form of the Garrett-Munk model is used to compare these spectra with other internal wave observations. The GM model provides a statistical description of the "typical" internal wave observation because it is empirically derived. Specifically, we use the formulation of the spectrum presented by Munk (1981). Desaubies (1976) has shown that the four parameters of the GM model, E (nondimensional energy level), j_* (effective nondimensional mode number), b (vertical depth scale of N in m), and N_0 (buoyancy frequency scale in cph) can be conveniently recast into two independent parameters:

$$r = Eb^2N_0, \tag{1}$$

$$t = \frac{j_*}{2N_0b}. \tag{2}$$

The frequency spectra of vertical displacement and horizontal velocity can then be written

$$S_\zeta(\omega) = \frac{2}{\pi} r \frac{f}{N} \frac{(\omega^2 + f^2)^{1/2}}{\omega^3}, \tag{3}$$

$$S_u(\omega) = S_{u_1} + S_{u_2} = 8\pi rfN \frac{(\omega^2 + f^2)}{\omega^3(\omega^2 - f^2)^{1/2}}, \tag{4}$$

where frequency is expressed in cycles per hour (cph). The vertical displacement and horizontal-velocity spectral levels are proportional to $1/N$ and N respectively, consistent with WKB scaling. Both spectra, and hence the total energy, are scaled by the parameter r. At high frequency, $\omega \gg f$, the frequency dependence is ω^{-2}.

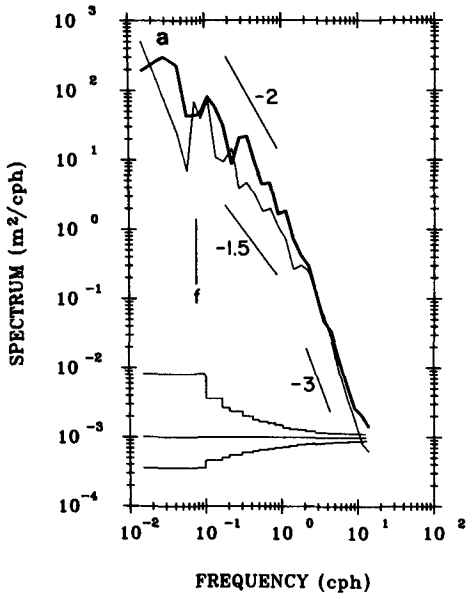

FIG. 4. (a) Autospectra of isotherm displacement for the −0.8° (thin line) and 1.6° (bold line) isotherms which oscillated at average depths of 67 and 137 m respectively. The 95% confidence limits are also plotted. (b) Vertical velocity spectra converted from the displacement spectra plotted in (a) by multiplying by frequency-squared. (c) As in (b) but multiplied by the local buoyancy frequency, N (67 m) = 4.1 cph and N (137 m) = 2.5 cph. Note that the difference between the two spectra in the internal wave band shown in (b) is reduced when scaled by N. The Garrett-Munk spectrum is shown for reference. The 95% confidence limits are also plotted.

For reference the GM spectrum (Eq. 3) is plotted with the observations (Fig. 4c). The level of the spectrum is set from the canonical GM value of r = 320 m² cph, obtained by using the values of $E = 6.3 \times 10^{-5}$, b = 1300 m and N_0 = 3 cph (Garrett and Munk, 1975). The GM spectrum is similar in shape but significantly higher in level than the data (Fig. 4c). A quantitative measure of the observed spectral level was obtained by fitting the GM spectral

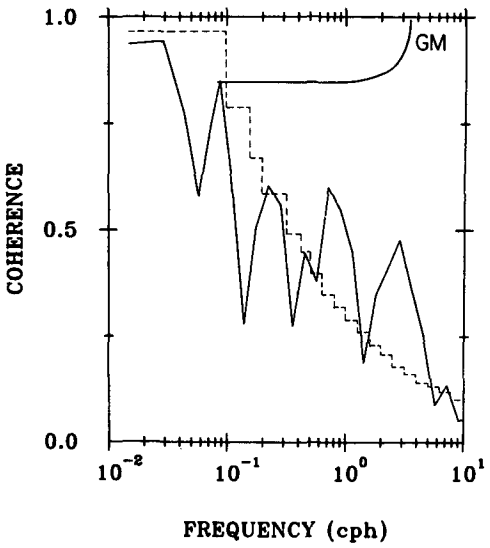

FIG. 5. Vertical coherence between the −1.4° isotherm at 57 m and the −0.4° isotherm at 76 m. Values above the dashed line are nonzero at the 95% significance level. Note the two peaks at 0.81 and 2.6 cph. The coherence from the GM model is also shown [Eq. (6)].

shape (Eq. 3) to the spectra in Fig. 4c by adjusting r so that the model variance equaled the variance in the data over the frequency band from 0.15 to 2.0 cph. The best-fit values of r are 47 and 75 m² cph from 67 and 137 m respectively. These values are significantly lower than the GM value.

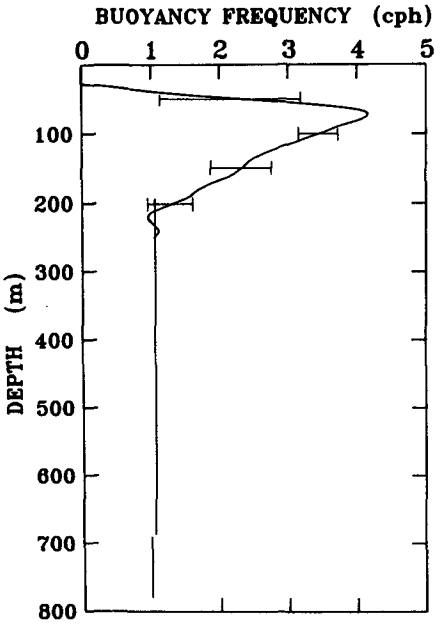

FIG. 6. Average buoyancy frequency profile. Values above 250 m are from measurements made with a CTD. Standard deviations of the 20 profiles used to form the average are shown at selected depths. Estimates from water samples are shown by vertical lines (Manley, personal communication, 1983).

To compare our results with historical observations, estimates of the internal-wave spectral energy from many experiments including other Arctic observations are plotted versus the local buoyancy frequency in Fig. 7a. These values were obtained from both horizontal velocity and vertical displacement data. A complete reference list is given in Table 1. The procedure for estimating the spectral levels varied among investigators; however, nearly all values were obtained by fitting the data to a frequency spectral slope approximating the GM model over a midfrequency range, far from the inertial, tidal and buoyancy frequencies. The spectral level was then converted to a value of r using (3) or (4) with the local values of f and N. Values of E, b, and N_0 were not estimated individually from the data—only the product $r = Eb^2N_0$ was estimated from the spectra. The quantity $r = Eb^2N_0$ is merely the GM notation of the spectral *level* after WKB scaling. If the GM model were truly universal, all observed values of r would lie on a horizontal line. As a group, the values from the Arctic are markedly lower than other observations; varying from factors of 3 to 70 below the canonical GM level. The values from midlatitude generally scatter within a factor of 3 of the GM level. High values occur near topographic features, e.g., Hydrographer Canyon (number 18), Hudson Canyon (number 21), Muir Seamount (number 17) and Ymir Ridge (number 13, highest two values). Values of r at low latitude also tend to be high, e.g., 16°N (number 10), 8.8°N (number 7) and 1.5°N (number 20a), and estimates very near the equator are too large to be plotted, e.g., 0 to 0.05°N (number 20b). Further discussion of the latitudinal scaling of the internal wave energy level is presented below.

What quantities should be considered "universal" in the GM parameterization of the spectrum? If E is constant, can variations in spectral level be described by variations in the stratification parameters b and N_0 alone? The quantities b and N_0 are introduced into the GM model as natural scales for length and time to non-dimensionalize the variables. It is unrealistic to expect that the complexity of internal wave interactions can be characterized by a single

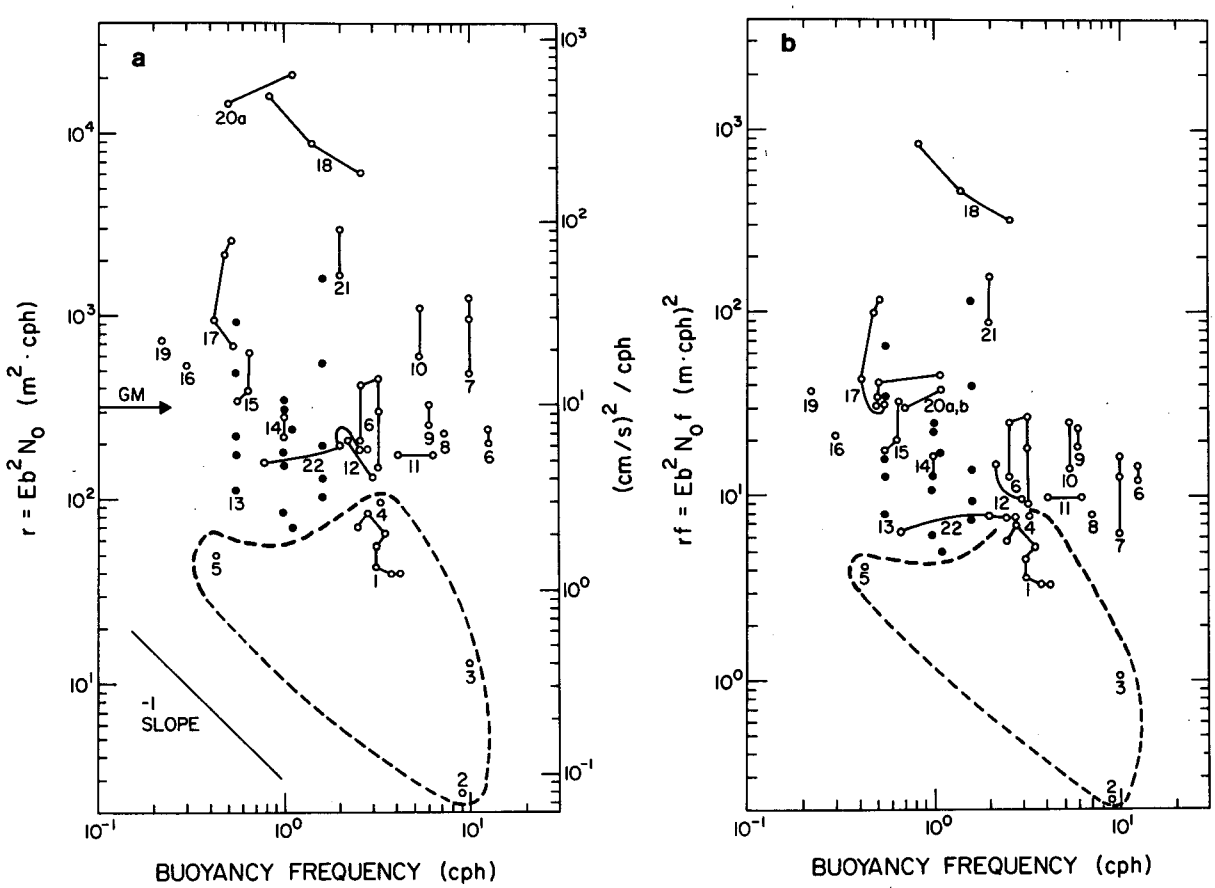

FIG. 7. (a) Estimates of the spectral level, reported in units of $r = Eb^2N_0$, are plotted vs local buoyancy frequency. The numbers refer to the data sources listed in Table 1. The estimates from the Arctic Ocean are enclosed by a dashed line. Lines with slope of −1 are isopleths of total internal-wave energy/volume. The solid dots belong to No. 13. (b) Same data as shown in (a) with ordinate rescaled by $r' = rf$ [m² cph²].

TABLE 1. Source of data displayed in Figs. 7a and 7b. The type of observation is indicated by the abbreviations T and V, representing temperature and velocity, respectively.

Number	Location (Lat. °N, Long. °W)	Primary and additional references	Data type	Duration, days	Instrument depth (m)	Water depth (m)
1	81.8, −4.0 Fram 3	This report Morison (1984)	T	4	50–150	800
2	75.4, 140.3 Ice Island T-3	Yearsley (1966) Morison (1984)	T	4	60	3000
3	85.0, 95.0 Ice Island T-3	Bernstein (1972) Morison (1984)	V	70	40, 60	
4	85.3, 97.8 Ice Island T-3	Neshyba *et al.* (1972) Morison (1984)	T	1	250	
5	89.2, 141.5 Arctic	Aagaard (1981)	V	35	1240, 1415	1500
6	46.6, 145.1 MILE, NE Pacific	Levine *et al.* (1983a)	T, V	19	30–175	4000
7	8.8, 22.9 GATE, Atlantic	Käse and Siedler (1980) Roth *et al.* (1981)	T, V	18–60	18–60	4900
8	25.0, 159.0 Pacific	Pinkel (1975) Roth *et al.* (1981)	T	10	110	4000
9	59.0, 12.5 JASIN, NE Atlantic	deWitt (1981) Levine *et al.* (1983b)	T	40	50	1500
10	16.0, 65.0 St. Croix	Tarbell *et al.* (1977) Roth *et al.* (1981)	T, V	32	95–243	
11	42.0, 70.0 Cape Cod	Zenk and Briscoe (1974) Roth *et al.* (1981)	T, V	21	59, 84	500
12	59.0, 12.5 JASIN, NE Atlantic	Weller (1982) Weller and Halpern (1983)	V	33	82, 100	1550
13	JASIN Area NE Atlantic	Gould *et al.* (1984) Levine *et al.* (1983b)	V	27–52	200–1500	1500
14	46.6, 130.2 MATE, NE Pacific	Levine and Irish (1981)	T, V	23	880–1300	2200
15	38.3, 70.0 39.2, 69.0 Under Gulf Stream	Luyten (1977) Wunsch and Webb (1979)	V	230	200–280	3000
16	28.0, 69.6 MODE Center	Wunsch (1976) Wunsch and Webb (1979)	V		4000	5400
17	33.5, 62.5 Muir Seamounts	Wunsch (1976) Wunsch and Webb (1979)	V	150	2100–3000	3000–4400
18	39.9, 68.9 Hydrographer Canyon	Wunsch (1976) Wunsch and Webb (1979)	V		320–710	350–700
19	38.0, −5.0 Mediterranean	Perkins (1972) Wunsch and Webb (1979)	V	60	1200	2700
20a 20b	1.5, −53.0 0 to 0.05, −50 to −57 Indian Ocean	Wunsch and Webb (1979) Eriksen (1980)	V	60–200	1500, 3600 1500, 3600	5100 4700–5100
21	39.5, 72.3 Hudson Canyon	Hotchkiss and Wunsch (1982)	V	105	100–700	300–700
22	27.7, 69.9 IWEX	Briscoe (1975) Roth *et al.* (1981)	T, V	42	600–2050	6000

length and time scale. One would not expect that an increase in b by a factor of 2 would increase the spectrum by a factor of 4 as (3) suggests. We view the GM formulation as an empirical description rather than a predictive model with the spectral *level* scaled by r. The proper scaling of the spectral level undoubtedly depends on the yet unknown balance of the generation, nonlinear transfer and dissipation processes that maintain the internal wave field.

Instead of r it might be preferable to compare the observations with the total internal-wave energy per unit mass $\hat{E}$. The total kinetic plus potential energy integrated over all frequencies for the GM model in units of J kg^{-1} is

$$\hat{E} = (3600)^{-2} \times 8\pi r N(z) \cos^{-1}[f/N(z)], \qquad (5)$$

where the contribution to the kinetic energy from the vertical velocity has been neglected. For the usual case of f/N much less than 1, $\hat{E} = (3600)^{-2} \times 4\pi^2 rN$. The energy $\hat{E}$ is then proportional to r and N and independent of f. Note that lines of constant $\hat{E}$ are indicated by -1 slope on Fig. 7a. Therefore the total energy levels observed in the upper Arctic Ocean (numbers 1–4) are comparable to some deep-ocean values. However, at comparable values of N, the Arctic values are still lower than at mid-latitude. The only observation from the deep Arctic Ocean (number 5) yields the lowest $\hat{E}$ on the figure.

4. Coherence

Estimates of coherence between vertically separated isotherm depths are only significantly different from zero in two frequency bands centered around 0.81 and 2.6 cph (Fig. 5). In the GM model the moored vertical coherence (MVC) is independent of frequency and is a function only of vertical separation Δ, and the bandwidth parameter t. The form given by Desaubies (1976) is

$$\mathrm{MVC}(\omega) = \exp[-2\pi t\Delta(N^2 - \omega^2)^{1/2}], \qquad (6)$$

where the approximation made by GM that $(N^2 - \omega^2) \approx N^2$ has not been made, resulting in a rise in coherence near N. The coherence level for the GM value of the parameter $t = 3.8 \times 10^{-4}$ cpm/cph is shown with the data in Fig. 5. The observations do not agree with the model. The statistically significant observed values are much below the predicted, and the variation of coherence below N is not independent of frequency.

The frequency bands of high coherence at 0.81 and 2.6 cph (Fig. 5) were investigated in greater detail. The coherence and phase in these bands are plotted as a function of vertical distance from the $-1.4°$ isotherm at 57 m (Fig. 8). In the band centered around 0.81 cph, which corresponds to a period of 1.1–1.4 h, the coherence decreases with increasing

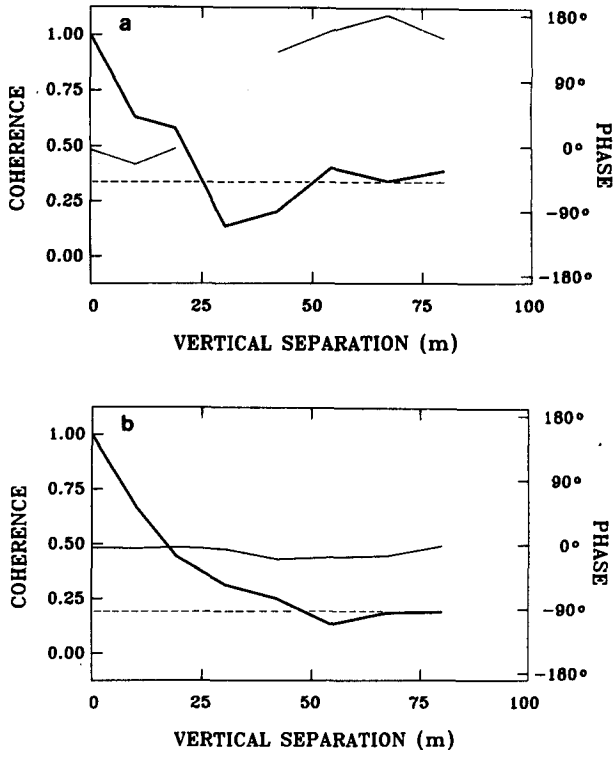

FIG. 8. Coherence (bold line) and phase (thin line) as a function of vertical separation from the mean depth of the $-1.4°$ isotherm at 57 m for frequency bands centered at (a) 0.81 and (b) 2.6 cph. Coherence was calculated between the $-1.4°$C and adjacent isotherms in increments of 0.2°. Coherence values above the dashed line are non-zero at the 95% significance level. Phase estimates are shown only where the coherence is significant.

separation until a 30 m separation is reached. At greater separation the coherence increases. The waves are nearly in phase between 57 and 76 m and then jump to nearly 180° out of phase between 57 m and depths deeper than 100 m. This pattern suggests a modal structure with a node located at the depth of the phase shift and coherence minimum, somewhere between 75 and 100 m. The structure of these waves can also be identified in the time series itself; examples of oscillations exhibiting this modal behavior are shown in Fig. 3.

Wavefunctions of vertical displacement $\Psi(z)$ were calculated by solving the boundary value problem

$$\Psi'' + k^2 \frac{(N^2 - \omega^2)}{(\omega^2 - f^2)} \Psi = 0 \qquad (7)$$

with $\Psi = 0$ at the top and bottom of the ocean. The wavefunctions at 0.81 cph for the lowest 4 modes are shown in Fig. 9. The shallowest nodes of modes 2–4 are in reasonable agreement with the depth of the observed phase change at 75–100 m. The cause of the high vertical coherence in this frequency band is not known; it has not been reported previously.

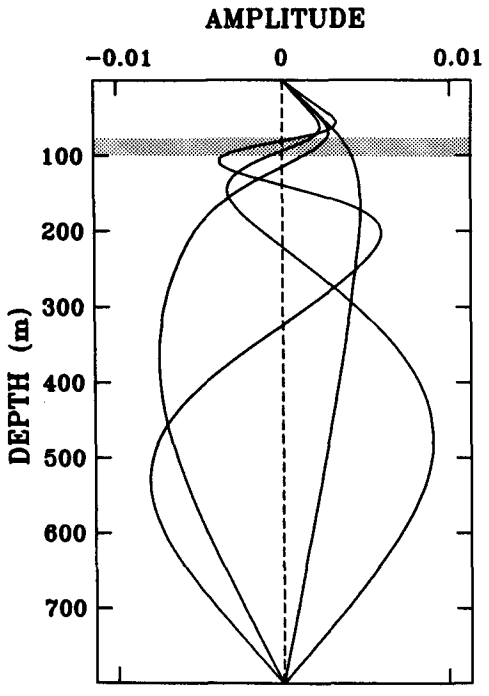

FIG. 9. Vertical wavefunctions for the first four modes at frequency 0.81 cph. A zero-crossing was observed in the data at this frequency at a depth of 75–100 m (shaded).

The coherence pattern at 2.6 cph, near the local value of N, is quite different; coherence decreases monotonically with vertical separation, and the oscillations are nearly in phase at all depths (Fig. 8b). Examples of these fluctuations are also shown in Fig. 3. Although in phase vertically, the scale of the vertical coherence is not large; the oscillations appear to be almost packet-like. This band of high vertical coherence, over the same frequency band as the break in spectral slope, is a feature often found in upper-ocean observations. It has been ascribed to fewer modes at those frequencies than the GM model prescribes (Levine *et al.*, 1983b).

5. *f*-scaling

The availability of internal wave observations from a wide range of latitudes provides an opportunity to test the dependence of the energy density on f in the GM model. It has been suggested by Munk (1981) that the f-scaling of the frequency spectral density be eliminated from the GM model. To test the validity of this suggestion, the same data from Fig. 7a are replotted as a function of

$$r' = rf \text{ m}^2 \text{ cph}^2 \tag{8}$$

in Fig. 7b. The scatter among the points is significantly reduced. Most noticeably affected are the low-latitude values, from GATE (9°N) and near St. Croix (16°N). The values near large topography are still large, and the low values from the Arctic remain distinct. Therefore, based on this survey of data, it appears reasonable to eliminate f in the scaling of the energy level, while retaining it as the lower limit of the internal-wave frequency band. This modification implies that the internal-wave energy per unit mass $\hat{E}$ is proportional to $1/f$ while the level of the frequency spectrum is independent of f. Further research is needed to determine if the hypothesis of constant spectral level is consistent with the dynamics controlling the energy flow through the internal wave field.

We have indicated that scaling by r' is consistent with observations but have not attempted to reformulate the entire GM model. In contrast to the frequency spectrum this new scaling implies that both vertical and horizontal wavenumber spectra are proportional to $1/f$ (S. Hayes, personal communication, 1983). Therefore, wavenumber spectral levels would increase dramatically as the equator is approached, a feature that is not found in the data. A different formulation is needed to model values near the equator where the f-plane approximation is not valid; a model in the spirit of GM that treats equatorial waves has been developed by Eriksen (1980).

6. Summary and conclusions

Time series of temperature in the upper Arctic Ocean were measured by a thermistor chain hanging from the pack ice for five days in May 1981. The depths of isotherms were tracked in time; it is assumed that the variations in isotherm depth are primarily due to vertical displacement by internal waves.

Spectral analysis of vertical displacement provides a useful description of the internal wave field and allows direct comparison with the GM model and historical data. Between f (0.0825 cph) and N (2–4 cph) the frequency dependence is between $\omega^{-1.5}$ and ω^{-2} (Fig. 4a). This is slightly less steep than the GM model but consistent with other upper-ocean observations (Levine *et al.*, 1983b). Near N, the upper frequency limit for free internal waves, there is a sharp break in the spectral slope followed by a roll-off at higher frequency.

Significant vertical coherence in the internal-wave band occurs at two peaks at 0.81 and 2.6 cph. This does not follow the expectation of a uniform coherence level prescribed by the GM model (Fig. 5). The peak at 2.6 cph is characteristic of peaks found in other upper-ocean observations near local N, the frequency where the break in spectral slope is found (Levine *et al.*, 1983b). The pattern of both the coherence and phase of the oscillations at 0.81 cph indicates the presence of the shallowest node between 75 and 100 m. This is consistent with the location of a node in modes 2 to 4 of the vertical wavefunctions calculated from the mean N profile. The origin of this peak has not been determined. The large-scale circulation in

the region of the Yermak Plateau is complicated, and there are numerous fronts that could affect the propagation of internal waves. Perhaps this "high" mode peak is the result of interaction with the low-frequency flow; the lack of data prohibits even a qualitative assessment.

To put these observations into perspective, the energy level r of the internal waves is compared with results from historical data (Fig. 7a). There is considerable variation among the values. When the same data are re-scaled by multiplying by f, the scatter is much reduced (Fig. 7b). This supports the suggestion of Munk (1981) that the latitudinal scaling of the frequency spectral density should be eliminated from the GM model.

The most interesting result of this paper is that spectral levels determined from experiments in the Arctic Ocean are lower than the GM model and those measured at lower latitudes (Fig. 7a). However, one must be cautious in assessing significance. Because the time series are short, some of the ascribed geographical variation may be due to the temporal variability of the internal wave field. Recent multiyear observations in the Sargasso Sea during LOTUS (Long Term Upper Ocean Study) show fluctuations from a half or a third to two or three times the mean energy (Briscoe and Weller, 1984). Perhaps this five-day experiment occurred during a relatively calm period; however, it is more significant that all of the Arctic observations tend to be low compared to spectral levels at lower latitudes. Whether the variations are predominantly geographical or temporal awaits additional observations.

The Arctic observations invite speculation about possible reasons for the relatively low energy levels. The Arctic may be a place where deviations of internal waves from universality can elucidate sources and sinks of internal wave energy. Perhaps the lower energy can be related to the unique forcing and dissipation processes that are present in the Arctic:

1) The ice cover damps the internal wave field via a turbulent boundary layer.

2) Surface forcing is weaker owing to weaker winds and to the loss of momentum to the coast by internal ice stress.

3) The nature of the stress transfer through the ice is different from an ice-free ocean. The generation of internal waves may depend critically on the geometry of the underside of the ice; momentum transfer from surface waves to internal waves is not possible.

4) The internal tides which may transfer energy to other frequency bands in the temperate oceans are generally small in the Arctic or are not able to propagate as free waves (north of 75°N).

The significance of these processes in shaping the internal wave field is not yet known; additional investigations are needed.

Acknowledgments. We thank R. Baumann for his careful processing of the data and S. Gard for his assistance with the preparation of the figures. The support by the Office of Naval Research under codes 422PO (Levine and Paulson) and 425AR (Morison) is gratefully acknowledged.

REFERENCES

Aagaard, K., 1981: On the deep circulation in the Arctic Ocean. *Deep-Sea Res.*, **28A**, 251–268.

Bernstein, R. L., 1972: Observations of currents in the Arctic Ocean. Tech. Rep. No. 7, Contract N-00014-67-A-0108-0016. Lamont-Doherty Geological Observatory of Columbia University, Palisades, NY.

Briscoe, M. G., 1975: Preliminary results from the trimoored internal wave experiment (IWEX). *J. Geophys. Res.*, **80**, 3872–3884.

——, and R. A. Weller, 1984: Preliminary results from the Long-Term Upper-Ocean Study (LOTUS). *Dyn. Atmos. Oceans*, **8**, 243–265.

Coachman, L. K., and K. Aagaard, 1974: Physical oceanography of Arctic and subarctic seas. *Marine Geology and Oceanography of the Arctic Seas*, Y. Herman, Ed., Springer-Verlag, 1–72.

Desaubies, Y. J. F., 1976: Analytical representation of internal wave spectra. *J. Phys. Oceanogr.*, **6**, 976–981.

deWitt, L. M., 1981: Variability of the upper ocean internal wave field during JASIN. M.S. thesis, School of Oceanography, Oregon State University, Corvallis, OR.

Eriksen, C. C., 1980: Evidence for a continuous spectrum of equatorial waves in the Indian Ocean. *J. Geophys. Res.*, **85**, 3285–3303.

——, 1982: Observations of internal wave reflection off sloping bottoms. *J. Geophys. Res.*, **87**, 525–538.

Garrett, C. J. R., and W. Munk, 1972: Space-time scales of internal waves. *Geophys. Fluid Dyn.*, **2**, 255–264.

——, and ——, 1975: Space-time scales of internal waves: A progress report. *J. Geophys. Res.*, **80**, 291–297.

Gould, W. J., A. N. Cutler and D. Weddell, 1984: (Internal report, in preparation). Institute of Ocean Sciences, Wormley, England.

Hotchkiss, F. S., and C. Wunsch, 1982: Internal waves in Hudson Canyon with possible geological implications. *Deep-Sea Res.*, **29**, 415–442.

Jackson, H. R., G. L. Johnson, E. Sundvor and A. M. Myhre, 1984: The Yermak Plateau: Formed at a triple junction. *J. Geophys. Res.*, **89**, 3223–3232.

Käse, R. H., and G. Siedler, 1980: Internal wave kinematics in the upper tropical Atlantic. *Deep-Sea Res.*, **26** (Suppl), 161–189.

Levine, M. D., 1983: Internal waves in the ocean: A review. *Rev. Geophys. Space Phys.*, **21**, 1206–1216.

——, and J. D. Irish, 1981: A statistical description of temperature finestructure in the presence of internal waves. *J. Phys. Oceanogr.*, **11**, 676–691.

——, R. A. deSzoeke and P. P. Niiler, 1983a: Internal waves in the upper ocean during MILE. *J. Phys. Oceanogr.*, **13**, 240–257.

——, C. A. Paulson, M. G. Briscoe, R. A. Weller and H. Peters, 1983b: Internal waves in JASIN. *Phil. Trans. Roy. Soc. London*, **A308**, 389–405.

Luyten, J. R., 1977: Scales of motion in the deep Gulf Stream and across the Continental Rise. *J. Mar. Res.*, **35**, 49–74.

Morison, J. H., 1980: Forced internal waves in the Arctic Ocean. Ph.D. dissertation, Tech. Rep. Ref. M80-10, University of Washington, Seattle, WA.

——, 1984: Internal waves in the Arctic Ocean: A review. *Geophysics of Sea Ice*, N. Untersteiner, Ed. (In press).

Müller, P., D. J. Olbers and J. Willebrand, 1978: The Iwex spectrum. *J. Geophys. Res.*, **83**, 479–500.

Munk, W., 1981: Internal waves and small-scale processes. *Evolution of Physical Oceanography,* B. A. Warren and C. Wunsch, Eds., MIT Press, 264–290.

Neshyba, S. J., V. T. Neal and W. W. Denner, 1972: Spectra of internal waves: *In situ* measurements in a multiple-layered structure. *J. Phys. Oceanogr.,* **2,** 91–95.

Olbers, D. J., 1983: Models of the oceanic internal wave field. *Rev. Geophys. Space Phys.,* **21,** 1567–1606.

Perkins, H., 1972: Vertical oscillations in the Mediterranean. *Deep-Sea Res.,* **19,** 289–296.

Pinkel, R., 1975: Upper ocean internal wave observations from FLIP. *J. Geophys. Res.,* **80,** 3892–3910.

——, 1981: Observations of the near-surface internal wavefield. *J. Phys. Oceanogr.,* **11,** 1248–1257.

Roth, M. W., M. G. Briscoe and C. H. McComas, III, 1981: Internal waves in the upper ocean. *J. Phys. Oceanogr.,* **11,** 1234–1247.

Tarbell, S., S. Payne and R. Walden, 1977: A compilation of moored current meter data and associated mooring action data from mooring 592. Vol XIV (1976 Data), WHOI-77-41, Woods Hole Oceanographic Institution, 122 pp.

Weller, R. A., 1982: The relation of near-inertial motions observed in the mixed layer during the JASIN (1978) experiment to the local wind stress and to the quasi-geostrophic flow field. *J. Phys. Oceanogr.,* **12,** 1122–1136.

——, and D. Halpern, 1983: The velocity structure of the upper ocean in the presence of surface forcing and mesoscale oceanic eddies. *Phil. Trans. Roy. Soc. London,* **A308,** 327–340.

Wunsch, C., 1975: Deep ocean internal waves: what do we really know? *J. Geophys. Res.,* **80,** 339–343.

——, 1976: Geographical variability of the internal wave field: A search for sources and sinks. *J. Phys. Oceanogr.,* **6,** 471–485.

——, and S. Webb, 1979: The climatology of deep ocean internal waves. *J. Phys. Oceanogr.,* **9,** 235–243.

Yearsley, J. R., 1966: Internal waves in the Arctic Ocean. M.S. thesis, Mech. Eng. Dept., University of Washington, Seattle, WA.

Zenk, W., and M. G. Briscoe, 1974: The Cape Cod experiment on near-surface internal waves. WHOI Ref. 74-87, Woods Hole Oceanographic Institution, 52 pp.